# Determination of Proton-Coupled Electron Transfer Reorganization Energies with Application to Water Oxidation Catalysts

| | |
|---|---|
| Journal: | *Journal of the American Chemical Society* |
| Manuscript ID | ja-2019-01296b |
| Manuscript Type: | Communication |
| Date Submitted by the Author: | 06-Feb-2019 |
| Complete List of Authors: | Schneider, Jenny; University of North Carolina at Chapel Hill, Chemistry<br>Bangle, Rachel; University of North Carolina at Chapel Hill, Chemistry<br>Swords, Wesley; University of Wisconsin Madison Department of Chemistry, Chemistry<br>Troian-Gautier, Ludovic; University of North Carolina at Chapel Hill, Chemistry<br>Meyer, Gerald; University of North Carolina at Chapel Hill, Department of Chemistry; UNC Chapel Hill, Chemistry |
| | |

# Determination of Proton-Coupled Electron Transfer Reorganization Energies with Application to Water Oxidation Catalysts

Jenny Schneider, Rachel E. Bangle, Wesley B. Swords, Ludovic Troian-Gautier, and Gerald J. Meyer*

Department of Chemistry, University of North Carolina at Chapel Hill, Chapel Hill 27599, USA

*Supporting Information Placeholder*

**ABSTRACT:** The reorganization energy, $\lambda$, for interfacial electron transfer (ET) and for proton-coupled electron transfer (PCET) between a water oxidation catalyst and a conductive $In_2O_3$:Sn (ITO) oxide were extracted from kinetic data by application of Marcus-Gerischer theory. Specifically, light excitation of the water oxidation catalyst $[Ru^{II}(tpy)(bpy)_2(4,4'\text{-}(PO_3H_2)_2\text{-}bpy)OH_2]^{2+}$ ($Ru^{II}$-$OH_2$) anchored to a mesoporous thin film of ITO nanocrystallites, where tpy is 2,2':6',2''-terpyridine and bpy is 2,2'-bipyridine, resulted in rapid excited-state injection ($k_{inj} > 10^8$ $s^{-1}$). The subsequent reaction of the injected electron (ITO($e^-$)) and either the protonated or the deprotonated oxidized catalyst were quantified spectroscopically on nanosecond and longer time scales. The metallic character of the ITO allowed potentiostatic control of the reaction free energy change $-\Delta G^o$ over a 1 eV range. Below the p*K*a = 1.7 of the oxidized catalyst, the reaction was strictly ET and occurred much more rapidly than under more basic conditions. Over the pH range $2 \leq pH \leq 5$, the interfacial PCET reaction (ITO($e^-$) + $Ru^{III}$-OH + $H^+ \rightarrow$ $Ru^{II}$-$OH_2$) occurred on longer time scales than the ET reaction. Plots of the rate constants versus $-\Delta G^o$ provided a reorganization energy for PCET $\lambda_{PCET}$ = 0.9 eV and for ET $\lambda_{ET}$ = 0.5 eV. The generality of this approach was tested with a second water oxidation catalyst. The utilization of conductive oxides is shown to be a powerful tool for quantifying PCET reorganization energies at oxide surfaces for the first time.

Proton-coupled electron transfer (PCET) describes reactions that involve a change in both electron and proton content between reactants and products.[1–3] Inspired by natural photosynthesis, homogeneous reactions have been characterized.[4–10] The PCET reactivity at semiconducting[11,12] and metal interfaces[13–15] have also garnered considerable interest. Like electron transfer (ET) reactions, PCET dynamics are expected to depend on the electronic coupling, $H_{ab}$, the free energy change $-\Delta G^o$, and the reorganization energy $\lambda$, yet a consensus on the magnitude of $\lambda$ does not exist. Babcock intuitively predicted that protein reorganization would be smaller when the $H^+$ and the $e^-$ were transferred together as opposed to sequentially,[16,17] yet the limited experimental data available today suggests the opposite, $\lambda_{PCET} \geq \lambda_{ET}$.[5,18,19] As the outer-sphere reaction is likely to be a key determinant, it is desirable to determine $\lambda_{PCET}$ directly from kinetic data measured as a function of $-\Delta G^o$[20–22] as described by Marcus. Electrochemical techniques enable continuous tuning of $-\Delta G^o$ without the need to synthesize a family of donor-acceptor compounds. Herein, proof-of-principle examples of a new kinetic method are reported that utilize the transparent and conductive nature of highly doped oxide materials[23–25] with photoactive water oxidation catalysts that undergo well defined PCET chemistry[26–29]. Pulsed light excitation of the ruthenium catalysts results in rapid electron injection into the oxide yielding $Ru^{III}$-$OH_2$. Owing to the different p*K*a values of $Ru^{II}$-$OH_2$ (9.7) and $Ru^{III}$-$OH_2$ (1.7) the subsequent recombination reaction was tuned to be purely ET ($pH < 1.7$) or PCET ($2 \leq pH \leq 5$), though the latter can occur either in one concerted step (CPET) or sequentially, Scheme 1.[28] The data reveal clearly that PCET reactivity is kinetically inhibited relative to ET, behaviour shown to result from an almost two-fold increase in the reorganization energy. These experiments provide a new method by which $\lambda_{PCET}$ can be systematically quantified.

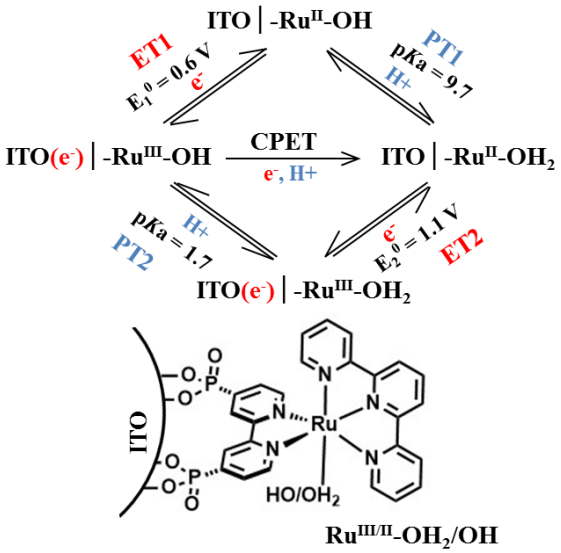


**Scheme 1.** Interfacial PCET following pulsed light excitation with possible sequential and concerted steps. The ET reaction was characterized at pH < 1.7, indicated as step ET2 and PCET at pH ≥ 2, respectively.

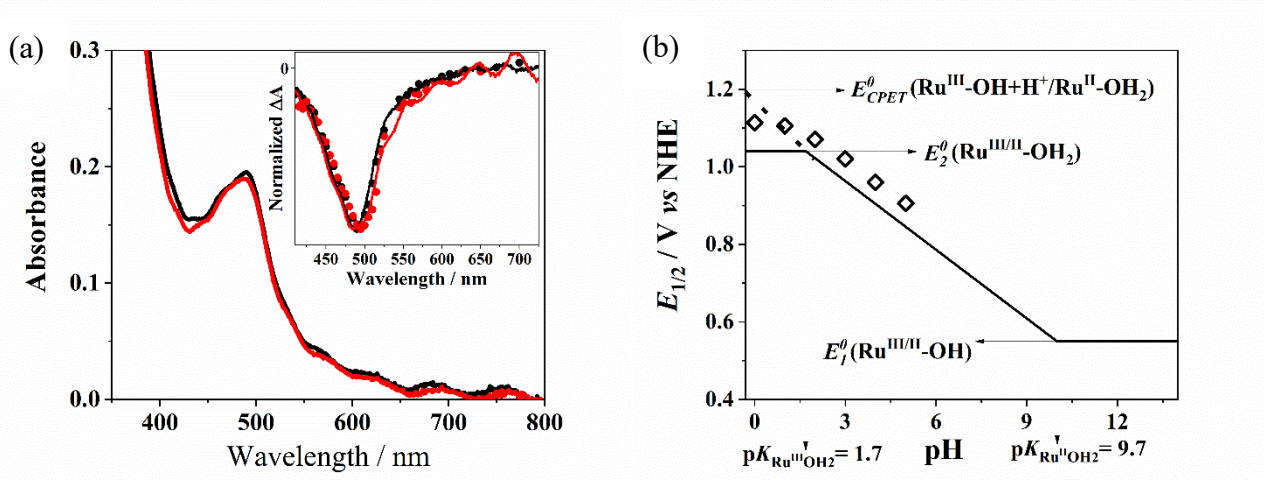


**Figure 1.** (a) The visible absorption spectra of ITO│-$Ru^{II}$-$OH_2$ recorded in a pH 1 (black) or pH 5 (red) solution. The inset shows the transient absorption spectra measured 20 ns after pulsed 532 nm excitation (4 mJ $cm^{-2}$) at pH 1 (black circles) and 5 (red circles) with overlaid simulations as the solid lines. (b) Plots of $E_{1/2}$ as a function of pH for the $Ru^{III/II}$ redox chemistry measured on the ITO surface (diamonds) and previously reported data (solid line) for the catalyst without phosphonate groups in fluid solution.[26] The p*K*a values for the oxidized and reduced catalyst, as well as the formal reduction potentials for the aquo $E^0_1$($Ru^{III/II}$-$OH_2$), hydroxo $E^0_2$ ($Ru^{III/II}$-OH), and for concerted $E^0_{CPET}$($Ru^{III}$-OH+$H^+$/$Ru^{II}OH_2$) are indicated.

The mesoporous degenerately-doped ITO films were prepared as previously reported[23] with a thin $ZrO_2$ shell deposited by atomic layer deposition to enable better time-resolution of the reaction kinetics[30] (see Supporting Information (SI)). Synthesis of [$Ru^{II}$(tpy)(bpy)$_2$(4,4'-($PO_3H_2$)$_2$-bpy)$OH_2$]$^{2+}$, where bpy is 2,2'-bipyridine and tpy is 2,2':6',2''-terpyridine, proceeded through a previously reported chloro analogue that was then treated with $AgNO_3$ in aqueous solutions.[29] Sensitization of the mesoporous ITO thin films was accomplished by overnight reaction in 5 μM aqueous catalyst solutions resulting in surface coverages of ~ 2 x $10^{-8}$ mol $cm^{-2}$, about ¼ of the saturation surface coverage, abbreviated ITO│- $Ru^{II}$-$OH_2$. The kinetic measurements were conducted with a previously described apparatus.[31] In some experiments [$Ru^{II}$(tpy)(4,4'-($CH_2$-$PO_3H_2$)$_2$-bpy)$OH_2$]$^{2+}$ was used.

Figure 1a shows the visible absorbance spectra of an ITO│-$Ru^{II}$-$OH_2$ electrode recorded in pH = 1 and 5 solutions. For both pH values a broad metal-to-ligand charge transfer (MLCT) absorption band centred at 490 nm was obtained. A quasi-reversible $E_{1/2}$($Ru^{III/II}$) redox wave was measured by cyclic voltammetry as a function of pH for the ITO anchored catalysts. As shown in Figure 1b, a Nernstian shift of 59 mV/pH was observed from pH = 5 to 1.7 indicative of a one-electron and one proton reaction. At pH values below 1.7, $E_{1/2}$($Ru^{III/II}$) was pH independent evincing the one-electron oxidation without proton involvement. Also shown as a solid line in Figure 1b are literature values for $E_{1/2}$ [$Ru^{III/II}$($OH_2$/OH)(tpy)(bpy)]$^{3+/2+}$ that display a small potential shift (< 50 mV) due to the absence of the electron withdrawing phosphonate groups.[26,28] Superimposed on this data are p*K*a values of $Ru^{II}$-$OH_2$ and $Ru^{III}$-$OH_2$, the formal reduction potentials for the aquo $E^0_1$($Ru^{III/II}$-$OH_2$) and the hydroxo $E^0_2$ ($Ru^{III/II}$-OH) catalyst. The reduction potemtial for concerted step $E^0_{CPET}$($Ru^{III}$-OH+$H^+$/$Ru^{II}OH_2$) was estimated following Saveant *et al*.[32,33]

The inset of Figure 1a shows transient spectra measured 20 ns after pulsed 532 nm laser excitation of ITO│- $Ru^{II}$-$OH_2$ in pH 1 and 5 solutions with overlaid simulations based on the $Ru^{II}$ and $Ru^{III}$ absorbance spectra. The prompt bleach of the MLCT absorption was consistent with rapid excited state injection $k_{inj}$ > $10^8$ $s^{-1}$ and the formation of an injected electron and oxidized catalyst: ITO($e^-$)│- $Ru^{III}$-$OH_2$/OH at pH 1 and 5. Transient absorption spectra alone did not report on the protonation state of the coordinated water. For all conditions of pH or $D_2O$, one interfacial state was observed transiently that recombined cleanly to ground-state products without evidence of permanent photochemistry.

Recombination of the injected electrons with the oxidized catalyst was measured as a function of the applied potential, $E_{app}$, and pH in a standard three-electrode cell. The recombination kinetics were measured over the potential range -0.1 to +0.9 V *vs* NHE in 100 meV increments. As indicated in Scheme 1 the recombination reaction could be tuned by pH to occur without (pH < 1.7) or with (pH ≥ 2) proton involvement. Figure 2 shows single-wavelength kinetic data on nanosecond and longer time scales for ET at pH 1 and PCET at pH 3, respectively.

The transient data were not well described by a first-order kinetic model as it is commonly observed on oxide surfaces, so the reciprocal of the time required for ½ of the charge separated states to recombine was taken as the rate constant $k_{1/2}$.[23,34,35] The $k_{1/2}$ values measured at different pH values are represented as function of $E_{app}$ in the inset of Figure 2. We note that the conclusion drawn herein was insensitive to kinetic analysis utilized the time necessary for the concentration to decrease to 1/e of the original value rather than $t_{1/2}$. For all pH values $k_{1/2}$ increased with $E_{app}$ reaching a limiting value $k_{1/2}^{max}$. In addition, recombination was significantly faster at pH = 0 (data not shown) and pH =1 than under less acidic conditions for $E_{app}$ > 200 mV, where the PCET reactivity was evident. To our knowledge, such a clear differentiation of interfacial recombination kinetics for ET and PCET reactions has been demonstrated here for the first time.

These kinetic experiments were repeated in $D_2O$ to determine the kinetic isotope effect (KIE) by relating the rate constants obtained in $H_2O$ $k_H$ to that in $D_2O$ $k_D$. At pH ≥ 2, a KIE = 1.1 was measured, Figure S1, where at pH ≤ 1 there was no significant isotope effect.

The reduction of $Ru^{III}$-OH to yield ground state products can occur either *via* concerted[15,27,36,37] or stepwise[13,14] mechanisms as

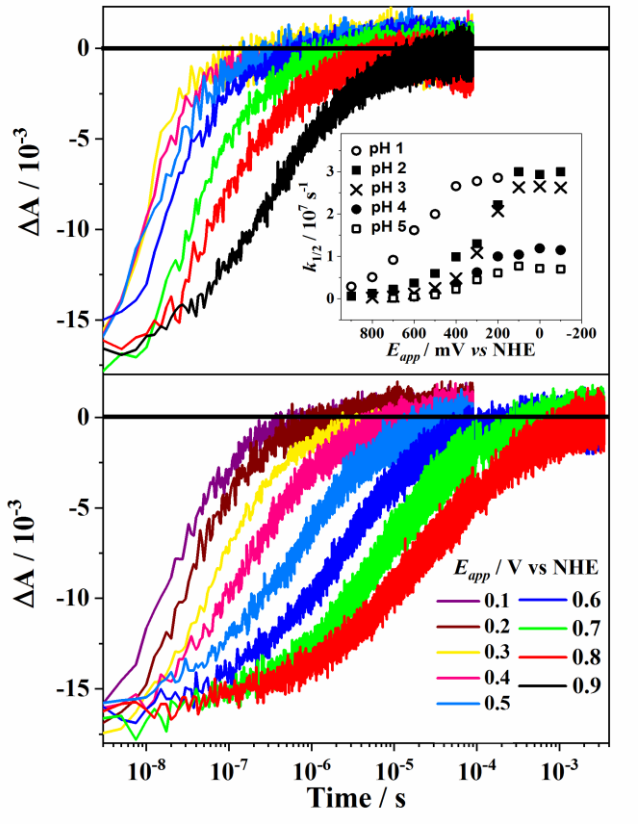


**Figure 2.** Absorption changes monitored at 490 nm after pulsed 532 nm laser excitation of ITO | -$Ru^{II}$-$OH_2$ as function of $E_{app}$ at pH 1 (top) and at pH 3 (bottom). The $k_{1/2}$ values obtained at different pH values are shown as function of $E_{app}$ in the inset.

shown in Scheme 1. Except for a few examples,[38,39] when electron transfer is rate limiting, the kinetics depend on driving force. Likewise, when proton transfer is rate limiting, the kinetics depend only on pH. Hence, the observation of both pH and bias (i.e. $-\Delta G^o$) dependent kinetics suggests the occurrence of CPET for reactions at pH ≥ 2. We note also that KIE values for CPET reactions are known to vary between 1-700.[8,40–43]

By analogy to heterogeneous ET reactions, the free energy dependence of the PCET kinetic data was analyzed with Marcus-Gerischer theory, illustrated in Scheme 2, that provides a mathematical framework to describe electron transfer between the electronic states of an electrode and a molecular reactant with the rate constant $k$ defined as:[44]

$$k = \frac{2\pi}{\hbar}\int_{-\infty}^{\infty} g(E) f(E, E_F) |H_{ab}(E)|^2 W(E) dE \qquad (1)$$

The total distribution of electronic levels in the ITO electrode is represented by $g(E)$ and their occupancy is controlled by $E_{app}$ which sets the Fermi energy, $E_F$. Because the high carrier density of ITO provides metallic character, $g(E)$ has been shown to be continuous with energy and ET/PCET occur isoenergetically. The quantity $f(E, E_F)$ is the Fermi-Dirac distribution, i.e. the probability that a state of energy $E$ is occupied by an electron and $H_{ab}(E)$ is the electronic coupling matrix element. The catalyst acceptor

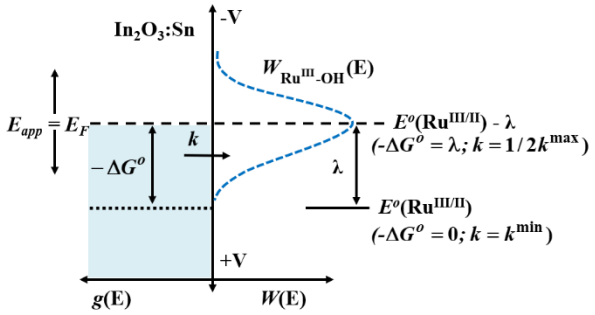


**Scheme 2.** A Gerischer-diagram representation of energetics associated with the PCET from ITO to $Ru^{III}$-OH to yield $Ru^{II}OH_2$. This reaction is expected for 2 ≤ pH ≤ 5.

states are represented by $W(E)$, a Gaussian distribution of classical activation energies:[45]

$$W(E) = \frac{1}{\sqrt{4\pi\lambda k_B T}} exp\left(\frac{-(\Delta G^o + \lambda)^2}{4\lambda k_B T}\right) \qquad (2)$$

where $\Delta G^o$ corresponds to the difference between $E_F$ and the standard reduction potential $E^0$, which corresponds to $E_{CPET}{}^0$ for the PCET reactions (see Figure 1b).

In the low-temperature limit of the Fermi-Dirac distribution and with the assumption that $g(E)$ and $H_{ab}(E)$ are independent of the applied potential, Equations 1 and 2 give:

$$k = k^{max}\int_{E_F}^{\infty} \frac{1}{\sqrt{4\pi\lambda k_B T}} exp\left(\frac{-(\Delta G^0 + \lambda)^2}{4\lambda k_B T}\right) dE \qquad (3)$$

$$\frac{k}{k^{max}} = \frac{1}{2}\left[1 - \mathrm{erf}\left(\frac{\Delta G^o + \lambda}{2\sqrt{\lambda k_B T}}\right)\right] \qquad (4)$$

Marcus-Gerischer theory predicts an increase in rate constant with increasing $-\Delta G^o$, but because of the continuum of the electronic states in ITO, the rate constants are expected to reach a maximum plateau when $-\Delta G^o > 2\lambda$. This is in contrast to the inverted region predicted by Marcus for molecular electron transfer reactions.[45] In addition, at the condition $-\Delta G^o = \lambda$, $k$ is not maximized but is equal to ½ $k^{max}$ as indicated in Scheme 2.

Plots of $k/k^{max}$ ($k = k_{1/2}$, $k^{max} = k_{1/2}{}^{max}$) as function of driving force are shown in Figure 3a for both ET (black) and PCET (blue). As expected, $k$ increases with $-\Delta G^o$ until a maximum value is realized. Fits of the experimental data to Equation 4 give $\lambda_{ET}$ = 0.5 eV and $\lambda_{PCET}$ = 0.9 eV. The corresponding $W(E)$ functions are shown in Figure 3b. To test generality, a derivative with a methylene spacer between the catalyst and the phosphonate binding group $[Ru^{II}(tpy)(4,4'\text{-}(CH_2\text{-}PO_3H_2)_2\text{-}bpy)OH_2]^{2+}$ was analysed in this manner to yield $\lambda_{ET}$ of 0.4 eV and $\lambda_{PCET}$ of 0.8 eV (Figure S2). Prior literature reports $\lambda_{PCET}$ > 1 eV in homogeneous solutions[18,22,46–48] and ~0.7 eV for heterogeneous interfaces[14]. Theoretical predictions by Hammes-Schiffer *et al.*[19,49] indicate an additional ~ 0.3 eV in reorganization for PCET relative to ET which is in a good agreement with the experimental value of 0.4 eV found here.

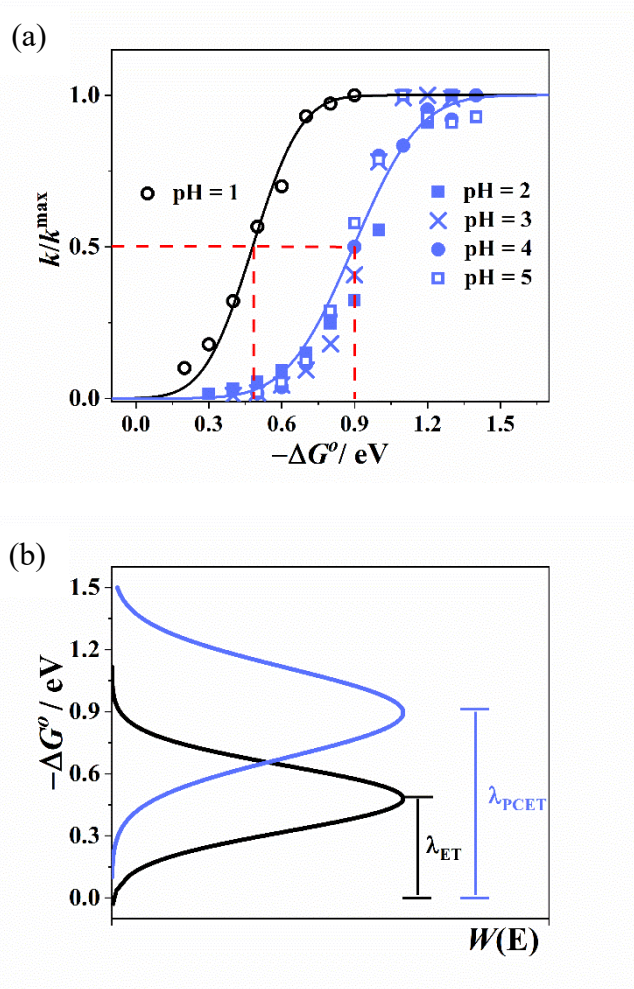


Figure 3. (a) Normalized rate constants (symbols) and fit to Equation 4 (solid lines) for ET (black) and PCET (blue). Dashed red lines represent the condition, $-\Delta G^o = \lambda$, at which $k = ½\ k^{max}$. (b) *W(E)* obtained from differentiation of the fit.

This study demonstrates a successful application of Marcus-Gerischer theory to experimentally quantify the reorganization energy for PCET reactions. The approach requires only a transparent conductor and a means to photo-initiate the PCET reaction. Future studies in which the PCET reactivity occurs to fully solvated species outside the electric double layer are expected to provide first-order kinetics[50] and a better understanding of how the oxide interface influences reorganization energies.[51] For the reduction of $Ru^{III}$-OH to $Ru^{II}$-$OH_2$ reported here, a concerted PCET pathway was identified that required 0.4 eV higher reorganization energy than did electron transfer without proton involvement. The decreased PCET recombination rates to water oxidation catalysts represents an important advance that indicates how solar water oxidation efficiencies may be enhanced at pH values where PCET reactivity is dominant.

## ASSOCIATED CONTENT

### Supporting Information

Experimental methods, kinetic isotope effect, Marcus-Gerischer analysis of kinetic data obtained with $[Ru^{II}(tpy)(4,4'\text{-}(CH_2\text{-}PO_3H_2)_2\text{-}bpy)OH_2]^{2+}$.

## AUTHOR INFORMATION

### Corresponding Author

*gjmeyer@email.unc.edu

### Notes

The authors declare no competing financial interests.

## ACKNOWLEDGMENT

This material is based upon work solely supported as part of the Alliance for Molecular PhotoElectrode Design for Solar Fuels (AMPED), an Energy Frontier Research Center (EFRC) funded by the U.S. Department of Energy, Office of Science, Office of Basic Energy Sciences under Award Number DE-SC0001011. This work made use of atomic layer deposition instrumentation at the Chapel Hill Analytical and Nanofabrication Laboratory (CHANL), a member of the North Carolina Research Triangle Nanotechnology Network (RTNN), which is supported by the National Science Foundation (Grant ECCS-1542015) as part of the National Nanotechnology Coordinated Infrastructure (NNCI). The authors thank Prof. Jillian Dempsey and Eric J. Piechota for the fruitful discussions and helpful suggestions.

## REFERENCES

(1) Dempsey, J. L.; Winkler, J. R.; Gray, H. B. Proton-Coupled Electron Flow in Protein Redox Machines. *Chem. Rev.* **2010**, *110*, 7024.

(2) Stubbe, J.; Nocera, D. G.; Yee, C. S.; Chang, M. C. Y. Radical Initiation in the Class I Ribonucleotide Reductase: Long-Range Proton-Coupled Electron Transfer? *Chem. Rev.* **2003**, *103*, 2167.

(3) Weinberg, D. R.; Gagliardi, C. J.; Hull, J. F.; Murphy, C. F.; Kent, C. A.; Westlake, B. C.; Paul, A.; Ess, D. H.; McCafferty, D. G.; Meyer, T. J. Proton-Coupled Electron Transfer. *Chem. Rev.* **2012**, *112*, 4016.

(4) Hammarström, L.; Styring, S. Proton-Coupled Electron Transfer of Tyrosines in Photosystem II and Model Systems for Artificial Photosynthesis: The Role of a Redox-Active Link between Catalyst and Photosensitizer. *Energy Environ. Sci.* **2011**, *4*, 2379.

(5) Sjödin, M.; Styring, S.; Åkermark, B.; Sun, L.; Hammarström, L. Proton-Coupled Electron Transfer from Tyrosine in a Tyrosine−Ruthenium−tris-Bipyridine Complex: Comparison with Tyrosine Z Oxidation in Photosystem II. *J. Am. Chem. Soc.* **2000**, *122*, 3932.

(6) Irebo, T.; Zhang, M.-T.; Markle, T. F.; Scott, A. M.; Hammarström, L. Spanning Four Mechanistic Regions of Intramolecular Proton-Coupled Electron Transfer in a $Ru(Bpy)_3^{2+}$–Tyrosine Complex. *J. Am. Chem. Soc.* **2012**, *134*, 16247.

(7) Mora, S. J.; Odella, E.; Moore, G. F.; Gust, D.; Moore, T. A.; Moore, A. L. Proton-Coupled Electron Transfer in Artificial Photosynthetic Systems. *Acc. Chem. Res.* **2018**, *51*, 445.

(8) Manbeck, G. F.; Fujita, E.; Concepcion, J. J. Proton-Coupled Electron Transfer in a Strongly Coupled Photosystem II-Inspired Chromophore–Imidazole–Phenol Complex: Stepwise Oxidation and Concerted Reduction. *J. Am. Chem. Soc.* **2016**, *138*, 11536.

(9) Hammes-Schiffer, S.; Stuchebrukhov, A. A. Theory of Coupled Electron and Proton Transfer Reactions. *Chem. Rev.* **2010**, *110*, 6939.

(10) Odella, E.; Mora, S. J.; Wadsworth, B. L.; Huynh, M. T.; Goings, J. J.; Liddell, P. A.; Groy, T. L.; Gervaldo, M.; Sereno, L. E.; Gust, D. Controlling Proton-Coupled Electron Transfer in Bioinspired Artificial Photosynthetic Relays. *J. Am. Chem. Soc.* **2018**, *140*, 15450.

(11) Braten, M. N.; Gamelin, D. R.; Mayer, J. M. Reaction Dynamics of Proton-Coupled Electron Transfer from Reduced ZnO Nanocrystals. *ACS Nano* **2015**, *9*, 10258.

(12) Valdez, C. N.; Schimpf, A. M.; Gamelin, D. R.; Mayer, J. M. Proton-Controlled Reduction of ZnO Nanocrystals: Effects of Molecular

Reductants, Cations, and Thermodynamic Limitations. *J. Am. Chem. Soc.* **2016**, *138*, 1377.

(13) Haddox, R. M.; Finklea, H. O. Proton-Coupled Electron Transfer of an Osmium Aquo Complex on a Self-Assembled Monolayer on Gold. *J. Phys. Chem. B* **2004**, *108*, 1694.

(14) Madhiri, N.; Finklea, H. O. Potential-, pH-, and Isotope-Dependence of Proton-Coupled Electron Transfer of an Osmium Aquo Complex Attached to an Electrode. *Langmuir* **2006**, *22*, 10643.

(15) Costentin, C.; Robert, M.; Savéant, J.-M.; Teillout, A.-L. Concerted and Stepwise Proton-Coupled Electron Transfers in Aquo/Hydroxo Complex Couples in Water: Oxidative Electrochemistry of $[Os^{II}(Bpy)_2(Py)(OH_2)]^{2+}$. *ChemPhysChem 10*, 191.

(16) Westphal, K. L.; Tommos, C.; Cukier, R. I.; Babcock, G. T. Concerted Hydrogen-Atom Abstraction in Photosynthetic Water Oxidation. *Curr. Opin. Plant Biol.* **2000**, *3*, 236.

(17) Tommos, C.; Babcock, G. T. Oxygen Production in Nature: A Light-Driven Metalloradical Enzyme Process. *Acc. Chem. Res.* **1998**, *31*, 18.

(18) Sjödin, M.; Styring, S.; Wolpher, H.; Xu, Y.; Sun, L.; Hammarström, L. Switching the Redox Mechanism: Models for Proton-Coupled Electron Transfer from Tyrosine and Tryptophan. *J. Am. Chem. Soc.* **2005**, *127*, 3855.

(19) Ghosh, S.; Soudackov, A. V; Hammes-Schiffer, S. Electrochemical Electron Transfer and Proton-Coupled Electron Transfer: Effects of Double Layer and Ionic Environment on Solvent Reorganization Energies. *J. Chem. Theory Comput.* **2016**, *12*, 2917.

(20) Huang, T.; Rountree, E. S.; Traywick, A. P.; Bayoumi, M.; Dempsey, J. L. Switching between Stepwise and Concerted Proton-Coupled Electron Transfer Pathways in Tungsten Hydride Activation. *J. Am. Chem. Soc.* **2018**, *140*, 14655.

(21) Nomrowski, J.; Wenger, O. S. Photoinduced PCET in Ruthenium–Phenol Systems: Thermodynamic Equivalence of Uni- and Bidirectional Reactions. *Inorg. Chem.* **2015**, *54*, 3680.

(22) Morris, W. D.; Mayer, J. M. Separating Proton and Electron Transfer Effects in Three-Component Concerted Proton-Coupled Electron Transfer Reactions. *J. Am. Chem. Soc.* **2017**, *139*, 10312.

(23) Farnum, B. H.; Morseth, Z. A.; Brennaman, M. K.; Papanikolas, J. M.; Meyer, T. J. Application of Degenerately Doped Metal Oxides in the Study of Photoinduced Interfacial Electron Transfer. *J. Phys. Chem. B* **2015**, *119*, 7698.

(24) Farnum, B. H.; Morseth, Z. A.; Lapides, A. M.; Rieth, A. J.; Hoertz, P. G.; Brennaman, M. K.; Papanikolas, J. M.; Meyer, T. J. Photoinduced Interfacial Electron Transfer within a Mesoporous Transparent Conducting Oxide Film. *J. Am. Chem. Soc.* **2014**, *136*, 2208.

(25) Farnum, B. H.; Morseth, Z. A.; Brennaman, M. K.; Papanikolas, J. M.; Meyer, T. J. Driving Force Dependent, Photoinduced Electron Transfer at Degenerately Doped, Optically Transparent Semiconductor Nanoparticle Interfaces. *J. Am. Chem. Soc.* **2014**, *136*, 15869.

(26) Concepcion, J. J.; Jurss, J. W.; Templeton, J. L.; Meyer, T. J. One Site is Enough. Catalytic Water Oxidation by $[Ru(Tpy)(Bpm)(OH_2)]^{2+}$ and $[Ru(Tpy)(Bpz)(OH_2)]^{2+}$. *J. Am. Chem. Soc.* **2008**, *130*, 16462.

(27) McHatton, R. C.; Anson, F. C. Electrochemical Behavior of $Ru(Trpy)(Bpy)(OH_2)^{3+}$ in Aqueous Solution and when Incorporated in Nafion Coatings. *Inorg. Chem.* **1984**, *23*, 3935.

(28) Takeuchi, K. J.; Thompson, M. S.; Pipes, D. W.; Meyer, T. J. Redox and Spectral Properties of Monooxo Polypyridyl Complexes of Ruthenium and Osmium in Aqueous Media. *Inorg. Chem.* **1984**, *23*, 1845.

(29) Trammell, S. A.; Wimbish, J. C.; Odobel, F.; Gallagher, L. A.; Narula, P. M.; Meyer, T. J. Mechanisms of Surface Electron Transfer. Proton-Coupled Electron Transfer. *J. Am. Chem. Soc.* **1998**, *120*, 13248.

(30) Kim, D. H.; Losego, M. D.; Peng, Q.; Parsons, G. N. Atomic Layer Deposition for Sensitized Solar Cells: Recent Progress and Prospects. *Adv. Mater. Interfaces* **2016**, *3*, 1600354.

(31) Argazzi, R.; Bignozzi, C. A.; Heimer, T. A.; Castellano, F. N.; Meyer, G. J. Enhanced Spectral Sensitivity from Ruthenium(II) Polypyridyl Based Photovoltaic Devices. *Inorg. Chem.* **1994**, *33*, 5741.

(32) Costentin, C.; Robert, M.; Savéant, J.-M. Concerted Proton−Electron Transfer Reactions in Water. Are the Driving Force and Rate Constant Depending on pH when Water Acts as Proton Donor or Acceptor? *J. Am. Chem. Soc.* **2007**, *129*, 5870.

(33) Bonin, J.; Costentin, C.; Robert, M.; Routier, M.; Savéant, J.-M. Proton-Coupled Electron Transfers: pH-Dependent Driving Forces? Fundamentals and Artifacts. *J. Am. Chem. Soc.* **2013**, *135*, 14359.

(34) Haque, S. A.; Tachibana, Y.; Klug, D. R.; Durrant, J. R. Charge Recombination Kinetics in Dye-Sensitized Nanocrystalline Titanium Dioxide Films under Externally Applied Bias. *J. Phys. Chem. B* **1998**, *102*, 1745.

(35) Clifford, J. N.; Palomares, E.; Nazeeruddin, M. K.; Grätzel, M.; Nelson, J.; Li, X.; Long, N. J.; Durrant, J. R. Molecular Control of Recombination Dynamics in Dye-Sensitized Nanocrystalline $TiO_2$ Films: Free Energy *vs* Distance Dependence. *J. Am. Chem. Soc.* **2004**, *126*, 5225.

(36) Lebeau, E. L.; Binstead, R. A.; Meyer, T. J. Mechanistic Implications of Proton Transfer Coupled to Electron Transfer. *J. Am. Chem. Soc.* **2001**, *123*, 10535.

(37) Chen, Z.; Vannucci, A. K.; Concepcion, J. J.; Jurss, J. W.; Meyer, T. J. Proton-Coupled Electron Transfer at Modified Electrodes by Multiple Pathways. *Proc. Natl. Acad. Sci.* **2011**, *108*, E1461.

(38) Lennox, J. C.; Dempsey, J. L. Influence of Proton Acceptors on the Proton-Coupled Electron Transfer Reaction Kinetics of a Ruthenium–Tyrosine Complex. *J. Phys. Chem. B* **2017**, *121*, 10530.

(39) Pizano, A. A.; Yanga, J.L.; Nocera, D. G. Energy Transfer Mediated by Asymmetric Hydrogen-Bonded Interfaces. *Chem. Scie.* **2012**, *3*, 455.

(40) Eisenhart, T. T.; Dempsey, J. L. Photo-Induced Proton-Coupled Electron Transfer Reactions of Acridine Orange: Comprehensive Spectral and Kinetics Analysis. *J. Am. Chem. Soc.* **2014**, *136*, 12221.

(41) Glover, S. D.; Parada, G. A.; Markle, T. F.; Ott, S.; Hammarström, L. Isolating the Effects of the Proton Tunneling Distance on Proton-Coupled Electron Transfer in a Series of Homologous Tyrosine-Base Model Compounds. *J. Am. Chem. Soc.* **2017**, *139*, 2090.

(42) Iordanova, N.; Hammes-Schiffer, S. Theoretical Investigation of Large Kinetic Isotope Effects for Proton-Coupled Electron Transfer in Ruthenium Polypyridyl Complexes. *J. Am. Chem. Soc.* **2002**, *124*, 4848.

(43) Edwards, S. J.; Soudackov, A. V; Hammes-Schiffer, S. Analysis of Kinetic Isotope Effects for Proton-Coupled Electron Transfer Reactions. *J. Phys. Chem. A* **2009**, *113*, 2117.

(44) Bard, A. J.; Faulkner, L. R. Electrochemical Methods: Fundamentals and Applications, 2nd Ed.; Willey: New York, 2001.

(45) Marcus, R. A. On the Theory of Oxidation-Reduction Reactions Involving Electron Transfer. I. *J. Chem. Phys.* **1956**, *24*, 966.

(46) Schrauben, J. N.; Cattaneo, M.; Day, T. C.; Tenderholt, A. L.; Mayer, J. M. Multiple-Site Concerted Proton–Electron Transfer Reactions of Hydrogen-Bonded Phenols Are Nonadiabatic and Well Described by Semiclassical Marcus Theory. *J. Am. Chem. Soc.* **2012**, *134*, 16635.

(47) Saveant, J.-M. Electrochemical Approach to Proton-Coupled Electron Transfers: Recent Advances. *Energy. Environ. Sci.* **2012**, *5*, 7718.

(48) Costentin, C.; Robert, M.; Saveant, J.-M. Concerted Proton–Electron Transfers in the Oxidation of Phenols. *Phys. Chem. Chem. Phys.* **2010**, *12*, 11179.

(49) Hammes-Schiffer, S. Controlling Electrons and Protons through Theory: Molecular Electrocatalysts to Nanoparticles. *Acc. Chem. Res.* **2018**, *51*, 1975.

(50) Sampaio, R. N.; Troian-Gautier, L.; Meyer, G. J. A Charge-Separated State that Lives for Almost a Second at a Conductive Metal Oxide Interface. *Angew. Chemie Int. Ed.* **2018**, *57*, 15390.

(51) Spitler, M. T. Effect of Nanometer-Sized Surface Morphology upon Electrochemical Kinetics. *Electrochim. Acta* **2007**, *52*, 2294.

TOC Use only:

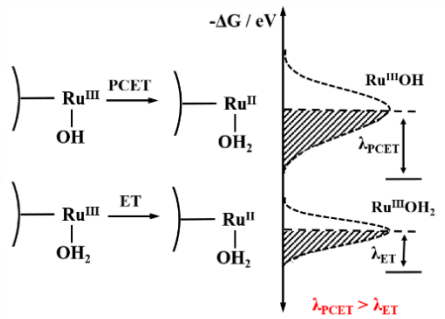
-ΔG / eV
Ru^III
OH
PCET
Ru^II
OH2
Ru^IIIOH
λPCET
Ru^III
OH2
ET
Ru^II
OH2
Ru^IIIOH2
λET
λPCET > λET